V. Dolejsi, M. Feistauer

A Semi-Implicit Discontinuous Galerkin Finite Element Method for the Numerical Solution of Inviscid Compressible Flow

Preprint No. MATH-knm-2003/2

25. 9. 2003

Submitted *J. Comput. Phys.*

Department of Numerical Mathematics, Faculty of Mathematics and Physics,
Charles University, Sokolovská 83, 186 75 Praha 8, Czech Republic

http://www.karlin.mff.cuni.cz/ms-preprints/

Cover print by Reprostředisko, Malostranské nám. 25, Praha 1 - Malá Strana
Design by Mirko Rokyta, picture of snowflake by Ondřej Kalenda
Current series administrator: V. Dolejsi

A Semi-Implicit Discontinuous Galerkin Finite Element Method for the Numerical Solution of Inviscid Compressible Flow [1]

Vít Dolejší, Miloslav Feistauer

Charles University Prague
Faculty of Mathematics and Physics
Sokolovská 83, 186 75 Praha 8
Czech Republic

Abstract

We deal with the numerical solution of an inviscid compressible flow with the aid of the discontinuous Galerkin finite element method. Since the explicit discretization of the time derivative requires a high restriction of the time step, we propose a semi-implicit time discretization approach. The homogeneity of inviscid fluxes allows us a simple linearization of the Euler equations which leads to a linear algebraic system. Numerical experiments performed for the Ringleb flow problem verify a higher order of accuracy of the presented method and demonstrate lower CPU-time costs in comparison with an explicit method.

Keywords: compressible Euler equations; homogeneity of inviscid fluxes; discontinuous Galerkin finite element method; implicit backward Euler method; Vijayasundaram numerical flux; semi-implicit linearized numerical scheme; CFL-stability condition; Ringleb test problem; experimental order of accuracy

1 Introduction

Our goal is to develop a sufficiently accurate, efficient and robust numerical method for the solution of an inviscid compressible flow, which is described by the system of the *Euler equations*. These nonlinear conservation laws have solutions with discontinuities and their approximations by conforming finite elements (FE) suffer from the Gibbs phenomenon. From this point of view, it seems that for conservation laws with discontinuous solutions, the finite volume (FV) method ([23], [14]) using piecewise constant approximations is more suitable, because the FV approximations are discontinuous on interelement interfaces, which allows better resolution of shock waves and contact discontinuities. On the other hand, the increase of accuracy in finite volume schemes applied on unstructured and/or anisotropic meshes seems to be problematic.

A combination of ideas and techniques of the FV and FE methods yields the *discontinuous Galerkin finite element method* (DGFEM) using advantages of both approaches

[1]This work was supported under the Grants No. 201/02/0684 and No. 201/00/D116 of the Czech Grant Agency and the Grant No. MSM 113200007 of the Ministry of Education of the Czech Republic. The authors acknowledge the support of these institutions.

and allowing to obtain schemes with a higher order accuracy in a natural way. DGFEM is based on the approximation of the solution of an initial-boundary value problem by piecewise polynomial functions over a finite element mesh without any requirement on interelement continuity. DGFEM was applied to nonlinear conservation laws already in 1989 by Cockburn and Shu ([7]). It was used for the numerical simulation of the compressible Euler equations later by Bassi and Rebay in [2]. During several recent years the DGFE schemes have been extensively developed and become more and more popular. Some aspects of the DGFEM and applications to gas dynamics are discussed in [1], [4], [10],[11], [13], [16], [12]. For a survey see, e. g. [6] and [8].

In [9] and [10] we developed a numerical method for the solution of the system of the Euler equations. The space discretization was carried out by the DGFEM and the forward Euler scheme was used for the time discretization. The resulting method is conditionally stable and the time step is drastically limited. The CFL number is larger for higher order Runge-Kutta time discretization, but it is more complicated and its use usually does not reduce the CPU time. To avoid this disadvantage it seems suitable to use an implicit method which allows to use a much longer time step. However, a fully implicit DGFEM leads to a large, strongly nonlinear algebraic system whose solution is rather complicated. This is the reason that we develop here a linearized semi-implicit DGFE scheme which appears quite efficient and robust.

The contents of the paper is the following. In Section 2, the initial-boundary value problem for the Euler equations is formulated and some properties of the Euler equations are mentioned. In Section 3, we carry out the discretization of the problem with the aid of a semi-implicit DGFEM. Section 4 contains a detailed description of the implementation of the method. Numerical examples demonstrating the accuracy and efficiency of the scheme are given in Section 5. The summary of results and outlook are discussed in Section 6.

2 Governing equations

The system of the Euler equations describing 2D inviscid flow can be written in the form

$$\frac{\partial \boldsymbol{w}}{\partial t} + \sum_{s=1}^{2} \frac{\partial \boldsymbol{f}_s(\boldsymbol{w})}{\partial x_s} = 0 \quad \text{in } Q_T = \Omega \times (0,T), \tag{2.1}$$

where $\Omega \subset I\!R^2$ is a bounded domain occupied by gas, $T > 0$ is the length of a time interval,

$$\boldsymbol{w} = (w_1, \ldots, w_4)^{\mathrm{T}} = (\rho,\, \rho v_1,\, \rho v_2,\, e)^{\mathrm{T}} \tag{2.2}$$

is the so-called *state vector* and

$$\begin{aligned} \boldsymbol{f}_s(\boldsymbol{w}) &= (f_s^1(w), \ldots, f_s^4(w)) \\ &= (\rho v_s,\, \rho v_s v_1 + \delta_{s1} p,\, \rho v_s v_2 + \delta_{s2} p,\, (e+p)\, v_s)^{\mathrm{T}}, \ s = 1, 2, \end{aligned} \tag{2.3}$$

are the so-called *inviscid (Euler) fluxes*. We use the following notation: ρ – density, p – pressure, e – total energy, $\boldsymbol{v} = (v_1, v_2)$ – velocity, δ_{sk} – Kronecker symbol (if $s = k$ then $\delta_{sk} = 1$, else $\delta_{sk} = 0$). The equation of state implies that

$$p = (\gamma - 1)\,(e - \rho|\boldsymbol{v}|^2/2). \tag{2.4}$$

Here $\gamma > 1$ is the Poisson adiabatic constant.

The system (2.1) – (2.4) is *hyperbolic*. It is equipped with the initial condition

$$\boldsymbol{w}(\boldsymbol{x}, 0) = \boldsymbol{w}^0(x), \quad x \in \Omega, \tag{2.5}$$

and the boundary conditions

$$B(\boldsymbol{w}) = 0 \quad \text{on } \partial\Omega \times (0, T), \tag{2.6}$$

chosen in such a way that problem (2.1) – (2.6) is linearly well–posed. (See, e.g. [19].) To this end, the boundary $\partial\Omega$ is formed by disjoint parts Γ_{IO} and Γ_W representing the inflow/outflow and impermeable walls, respectively. On Γ_W we prescribe the impermeability condition

$$\boldsymbol{v} \cdot \boldsymbol{n} = 0 \quad \text{on } \Gamma_W, \tag{2.7}$$

where $\boldsymbol{n}$ denotes the unit outer normal to $\partial\Omega$. In order to determine boundary conditions on Γ_{IO}, we define the matrix

$$\boldsymbol{P}(\boldsymbol{w}, \boldsymbol{n}) := \sum_{s=1}^{2} \boldsymbol{A}_s(\boldsymbol{w}) n_s, \tag{2.8}$$

where $\boldsymbol{n} = (n_1, n_2) \in I\!R^2$, $n_1^2 + n_2^2 = 1$ and

$$\boldsymbol{A}_s(\boldsymbol{w}) = \frac{D\boldsymbol{f}_s(\boldsymbol{w})}{D\boldsymbol{w}}, \quad s = 1, 2, \tag{2.9}$$

are the Jacobi matrices of the mappings $\boldsymbol{f}_s$. Then we prescribe m_n quantities characterizing the state vector $\boldsymbol{w}$, where m_n is the number of negative eigenvalues of the matrix $\boldsymbol{P}(\boldsymbol{w}, \boldsymbol{n})$ and extrapolate m_p quantities of $\boldsymbol{w}$ from interior of Ω, where $m_p = 4 - m_n$ is the number of nonnegative eigenvalues of $\boldsymbol{P}(\boldsymbol{w}, \boldsymbol{n})$. For details, see, e.g., [15] or [19].

Using relations (2.2) – (2.4), we express the fluxes $\boldsymbol{f}_s$, $s = 1, 2$, in terms of the variables $w_1, \ldots, w_4$ in the form

$$\boldsymbol{f}_s(\boldsymbol{w}) = \begin{pmatrix} w_{s+1} \\ \frac{w_{s+1} w_2}{w_1} + \delta_{s1}(\gamma - 1)\left(w_4 - \frac{w_2^2 + w_3^2}{2w_1}\right) \\ \frac{w_{s+1} w_3}{w_1} + \delta_{s2}(\gamma - 1)\left(w_4 - \frac{w_2^2 + w_3^2}{2w_1}\right) \\ \frac{w_{s+1}}{w_1}\left(\gamma w_4 - (\gamma - 1)\frac{w_2^2 + w_3^2}{2w_1}\right) \end{pmatrix}, \quad s = 1, 2. \tag{2.10}$$

Obviously, $\boldsymbol{f}_s$, $s = 1, 2$, are homogeneous mappings of order one, i.e.,

$$\boldsymbol{f}_s(\alpha \boldsymbol{w}) = \alpha \boldsymbol{f}_s(\boldsymbol{w}), \ \alpha \in I\!R, \ \alpha \neq 0, \ i = 1, 2. \tag{2.11}$$

Then it is easy to show (see [15], page 432) that

$$\boldsymbol{f}_s(\boldsymbol{w}) = \boldsymbol{A}_s(\boldsymbol{w}) \boldsymbol{w}, \ s = 1, 2. \tag{2.12}$$

3 Discretization

3.1 Broken Sobolev space

In what follows we use the standard notation for function spaces: $H^k(\Omega)$ is the Sobolev space and $C^1(0,T;X)$ is the space of continuously differentiable mappings on $[0,T]$ with values in X.

Let Ω_h be a polygonal approximation of Ω. In order to derive the discrete problem, we consider a mesh $\mathcal{T}_h$ of Ω_h consisting of various types of convex elements $K_i \in \mathcal{T}_h,\ i \in I$ (I is a suitable index set), e. g., triangles, quadrilaterals or in general convex polygons.

By Γ_{ij} we denote a common edge between two neighbouring elements K_i and K_j. The symbol $\boldsymbol{n}_{ij} = ((n_{ij})_1, (n_{ij})_2)$ denotes the unit outer normal to ∂K_i on the side Γ_{ij}. Moreover, we set $s(i) = \{j \in I; K_j \text{ is a neighbour of } K_i\}$. The boundary $\partial\Omega_h$ is formed by a finite number of faces of elements K_i adjacent to $\partial\Omega_h$. We denote all these boundary faces by S_j, where $j \in I_b \subset Z^- = \{-1,-2,\ldots\}$. Now we set $\gamma(i) = \{j \in I_b; S_j \text{ is a face of } K_i \in \mathcal{T}_h\}$ and $\Gamma_{ij} = S_j$ for $K_i \in \mathcal{T}_h$ such that $S_j \subset \partial K_i,\ j \in I_b$. For K_i not containing any boundary face S_j we set $\gamma(i) = \emptyset$. Obviously, $s(i) \cap \gamma(i) = \emptyset$ for all $i \in I$. Now, if we write $S(i) = s(i) \cup \gamma(i)$, we have

$$\partial K_i = \bigcup_{j\in S(i)} \Gamma_{ij}, \quad \partial K_i \cap \partial\Omega_h = \bigcup_{j\in\gamma(i)} \Gamma_{ij}. \tag{3.1}$$

Moreover, we define two subsets $\gamma_{IO}(i)$ and $\gamma_W(i)$ of $\gamma(i)$ such that faces $\Gamma_{ij},\ j \in \gamma_{IO}(i)$, approximate Γ_{IO} and $\Gamma_{ij},\ j \in \gamma_W(i)$, approximate Γ_W.

We define the so-called *broken Sobolev space*

$$H^k(\Omega,\mathcal{T}_h) = \{v; v|_K \in H^k(K)\ \forall\, K \in \mathcal{T}_h\}. \tag{3.2}$$

If $v \in H^k(\Omega,\mathcal{T}_h)$, then

$$v|_{\Gamma_{ij}} \neq v|_{\Gamma_{ji}}, \tag{3.3}$$

in general, where $v|_{\Gamma_{ij}}$ and $v|_{\Gamma_{ji}}$ denote the values of v on Γ_{ij} considered from the interior and the exterior of K_i, respectively.

In order to derive the discrete problem, we multiply (2.1) by a test function $\boldsymbol{\varphi} \in [H^1(\Omega,\mathcal{T}_h)]^4$ and integrate over any element $K_i,\ i \in I$. With the use of Green's theorem we obtain the integral identity

$$\begin{aligned} \frac{\partial}{\partial t}\int_{K_i} \boldsymbol{w}\cdot\boldsymbol{\varphi}\,\mathrm{d}\boldsymbol{x} &= \int_{K_i}\sum_{s=1}^{2} \boldsymbol{f}_s(\boldsymbol{w})\cdot\frac{\partial\boldsymbol{\varphi}}{\partial x_s}\,\mathrm{d}\boldsymbol{x} \\ &- \sum_{j\in S(i)}\int_{\Gamma_{ij}}\sum_{s=1}^{2} \boldsymbol{f}_s(\boldsymbol{w})\cdot\boldsymbol{\varphi}\, n_s\,\mathrm{d}S, \end{aligned} \tag{3.4}$$

where $\boldsymbol{n}_{ij} = (n_1, n_2)$ is the unit outer normal to element K_i. Summing (3.4) over all $K_i \in \mathcal{T}_h$, we obtain the identity

$$\begin{aligned} \frac{\partial}{\partial t}\sum_{K_i\in\mathcal{T}_h}\int_{K_i} \boldsymbol{w}\cdot\boldsymbol{\varphi}\,\mathrm{d}x &= \sum_{K_i\in\mathcal{T}_h}\int_{K_i}\sum_{s=1}^{2} \boldsymbol{f}_s(\boldsymbol{w})\cdot\frac{\partial\boldsymbol{\varphi}}{\partial x_s}\,\mathrm{d}x - \\ &- \sum_{K_i\in\mathcal{T}_h}\sum_{j\in S(i)}\int_{\Gamma_{ij}}\sum_{s=1}^{2} \boldsymbol{f}_s(\boldsymbol{w})\cdot\boldsymbol{\varphi}\, n_s\,\mathrm{d}S. \end{aligned} \tag{3.5}$$

This equality represents a weak form of the Euler equations in the sense of the broken Sobolev space $H^1(\Omega, \mathcal{T}_h)$.

3.2 Numerical solution

Now we shall introduce the discrete problem approximating identity (3.5) with the aid of the discontinuous Galerkin finite element method.

To evaluate the boundary integrals in (3.5) we use the approximation

$$\int_{\Gamma_{ij}} \sum_{s=1}^{2} \boldsymbol{f}_s(\boldsymbol{w}(t))\, n_s \cdot \boldsymbol{\varphi}\, \mathrm{d}S \approx \int_{\Gamma_{ij}} \boldsymbol{H}(\boldsymbol{w}(t)|_{\Gamma_{ij}}, \boldsymbol{w}(t)|_{\Gamma_{ji}}, \boldsymbol{n}_{ij}) \cdot \boldsymbol{\varphi}\, \mathrm{d}S, \tag{3.6}$$

where $\boldsymbol{H}$ is *the numerical flux*, $\boldsymbol{w}(t)|_{\Gamma_{ij}}$ and $\boldsymbol{w}(t)|_{\Gamma_{ji}}$ are the values of $\boldsymbol{w}$ on Γ_{ij} considered from the interior and the exterior of K_i, respectively, and at time t. It is necessary to specify the meaning of $\boldsymbol{w}(t)|_{\Gamma_{ji}}$ for $j \in \gamma(i)$. Taking into account the boundary conditions on Γ_{IO} described above, we prescribe m_n components of $\boldsymbol{w}$ on Γ_{ij} and extrapolate m_p components from the interior of K_i to Γ_{ij}. Thus, we define $\boldsymbol{w}|_{\Gamma_{ji}} = (w_1, w_2, w_3, w_4)|_{\Gamma_{ji}}$ by

$$w_l|_{\Gamma_{ji}} = \begin{cases} g_l & \text{if the } l\text{-th component of } \boldsymbol{w} \text{ is prescribed} \\ w_l|_{\Gamma_{ij}} & \text{if the } l\text{-th component of } \boldsymbol{w} \text{ is extrapolated} \end{cases}, \qquad l = 1, \ldots, 4, \quad j \in \gamma_{IO}(i), \tag{3.7}$$

where $\boldsymbol{g} = (g_1, g_2, g_3, g_4)$ is a given state vector. For details, see, e.g. [15] or [19].

If $j \in \gamma_W(i)$, then we use the impermeability condition (2.7) and replace (3.6) by the approximation

$$\int_{\Gamma_{ij}} \boldsymbol{H}(\boldsymbol{w}(t)|_{\Gamma_{ij}}, \boldsymbol{w}(t)|_{\Gamma_{ji}}, \boldsymbol{n}_{ij}) \cdot \boldsymbol{\varphi}\, \mathrm{d}S := \int_{\Gamma_{ij}} \boldsymbol{F}_W(\boldsymbol{w}(t), \boldsymbol{n}_{ij}) \cdot \boldsymbol{\varphi}\, \mathrm{d}S, \quad j \in \gamma_W(i), \tag{3.8}$$

where

$$\boldsymbol{F}_W(\boldsymbol{w}, \boldsymbol{n}) \equiv (0, pn_1, pn_2, 0)^{\mathrm{T}}. \tag{3.9}$$

The pressure p is expressed in the form

$$p = (\gamma - 1)\,(w_4 - (w_2^2 + w_3^2)/(2w_1)), \tag{3.10}$$

following from (2.4) and (2.2) and extrapolated on Γ_{ij} from K_i and $\boldsymbol{n} = (n_1, n_2) = \boldsymbol{n}_{ij}$.

Let us note that the choice of a suitable numerical flux plays an important role, particularly in finite volume schemes. We can mention, e.g., the well-known Steger-Warming, Van Leer, Roe and Vijayasundaram numerical fluxes or the numerical fluxes based on the direct Riemann solver of the Euler equations. (For more details and references, see [19] or [27]). As for efficiency and robustness, we can recommend the Osher-Solomon numerical flux (see [24], [26], [20] or [19], Section 3.4), which we applied with a great success, e.g., in [17], [18].

An approximate solution is sought at each time instant t as an element of the space of discontinuous piecewise polynomial functions

$$S_h \equiv S^{p,-1}(\Omega, \mathcal{T}_h) = \{v; v|_K \in P_p(K)\ \forall\, K \in \mathcal{T}_h\}, \tag{3.11}$$

where $p \geq 0$ is an integer and $P_p(K)$ denotes the space of all polynomials on K of degree $\leq p$. For $\boldsymbol{w}_h, \boldsymbol{\varphi}_h \in [S_h]^4$ we introduce the forms

$$
\begin{aligned}
(\boldsymbol{w}_h, \boldsymbol{\varphi}_h) &= \int_\Omega \boldsymbol{w}_h(\boldsymbol{x}) \cdot \boldsymbol{\varphi}_h(\boldsymbol{x})\, \mathrm{d}\boldsymbol{x}, \\
\tilde{b}_h(\boldsymbol{w}_h, \boldsymbol{\varphi}_h) &= -\sum_{K \in \mathcal{T}_h} \int_K \sum_{s=1}^{2} \boldsymbol{f}_s(\boldsymbol{w}_h(\boldsymbol{x})) \cdot \frac{\partial \boldsymbol{\varphi}_h(\boldsymbol{x})}{\partial x_s}\, \mathrm{d}\boldsymbol{x} \\
&+ \sum_{K_i \in \mathcal{T}_h} \sum_{j \in S(i)} \int_{\Gamma_{ij}} \boldsymbol{H}(\boldsymbol{w}(t)|_{\Gamma_{ij}}, \boldsymbol{w}(\boldsymbol{x})|_{\Gamma_{ji}}, \boldsymbol{n}_{ij}) \cdot \boldsymbol{\varphi}_h(\boldsymbol{x}) \mathrm{d}S.
\end{aligned}
\tag{3.12}
$$

We say that $\boldsymbol{w}_h$ is the *approximate solution* of (2.1), if it satisfies the conditions

$$
\begin{aligned}
&\text{a)} \quad \boldsymbol{w}_h \in C^1([0,T],[S_h]^4), \\
&\text{b)} \quad \frac{\mathrm{d}}{\mathrm{d}t}(\boldsymbol{w}_h(t), \boldsymbol{\varphi}_h) + \tilde{b}_h(\boldsymbol{w}_h(t), \boldsymbol{\varphi}_h) = 0 \quad \forall\, \boldsymbol{\varphi}_h \in [S_h]^4\ \forall\, t \in (0,T), \\
&\text{c)} \quad \boldsymbol{w}_h(0) = \Pi_h \boldsymbol{w}^0,
\end{aligned}
\tag{3.13}
$$

where $\Pi_h \boldsymbol{w}^0$ is the L^2-projection of $\boldsymbol{w}^0$ from the initial condition (2.5) on the space $[S_h]^4$. If we set $p = 0$, then we obviously obtain the finite volume method.

Relations (3.13) represent a system of ordinary differential equations which can be solved by a suitable numerical method. Usually, Runge-Kutta schemes are applied. Then we get conditionally stable methods applicable under a severe restriction of the length of the time step due to the CFL-stability condition. Since we are interested in numerical schemes not suffering from this drawback, we shall start from the time discretization by the implicit *backward Euler method*. To this end, we consider a partition $0 = t_0 < t_1 < t_2 \ldots$ of the time interval $(0,T)$ and set $\tau_k = t_{k+1} - t_k$. We use the notation $\boldsymbol{w}_h^k$ for the approximation of $\boldsymbol{w}_h(t_k)$. Then the *discrete problem* reads: for each $k \geq 0$ find $\boldsymbol{w}_h^{k+1}$ such that

$$
\begin{aligned}
&\text{a)} \quad \boldsymbol{w}_h^{k+1} \in [S_h]^4, \\
&\text{b)} \quad \left(\frac{\boldsymbol{w}_h^{k+1} - \boldsymbol{w}_h^k}{\tau_k}, \boldsymbol{\varphi}_h \right) + \tilde{b}_h(\boldsymbol{w}_h^{k+1}, \boldsymbol{\varphi}_h) = 0 \quad \forall\, \boldsymbol{\varphi}_h \in [S_h]^4, \quad k = 0, 1, \ldots, \\
&\text{c)} \quad \boldsymbol{w}_h^0 = \Pi_h \boldsymbol{w}^0.
\end{aligned}
\tag{3.14}
$$

Scheme (3.13) leads to a system of highly nonlinear algebraic equations whose numerical solution is rather complicated. In order to simplify the problem, in the following we shall linearize relation (3.13), b) and obtain a linear system.

3.3 Linearization

By (3.12), for $\boldsymbol{w}_h^{k+1}, \boldsymbol{\varphi}_h \in [S_h]^4$ we have

$$
\begin{aligned}
\tilde{b}_h(\boldsymbol{w}_h^{k+1}, \boldsymbol{\varphi}_h) &= \underbrace{-\sum_{K \in \mathcal{T}_h} \int_K \sum_{s=1}^{2} \boldsymbol{f}_s(\boldsymbol{w}_h^{k+1}(\boldsymbol{x})) \cdot \frac{\partial \boldsymbol{\varphi}_h(\boldsymbol{x})}{\partial x_s}\, \mathrm{d}\boldsymbol{x}}_{=:\tilde{\sigma}_1} \\
&+ \underbrace{\sum_{K_i \in \mathcal{T}_h} \sum_{j \in S(i)} \int_{\Gamma_{ij}} \boldsymbol{H}(\boldsymbol{w}_h^{k+1}(\boldsymbol{x})|_{\Gamma_{ij}}, \boldsymbol{w}_h^{k+1}(\boldsymbol{x})|_{\Gamma_{ji}}, \boldsymbol{n}_{ij}) \cdot \boldsymbol{\varphi}_h(\boldsymbol{x}) \mathrm{d}S}_{=:\tilde{\sigma}_2}.
\end{aligned}
\tag{3.15}
$$

The individual terms $\tilde{\sigma}_1$ and $\tilde{\sigma}_2$ will be linearized separately. For $\tilde{\sigma}_1$, we use the property (2.12) of the Euler fluxes and use the approximation

$$\tilde{\sigma}_1 \approx \sigma_1 = \sum_{K \in \mathcal{T}_h} \int_K \sum_{s=1}^{2} \boldsymbol{A}_s(\boldsymbol{w}_h^k(\boldsymbol{x}))\boldsymbol{w}_h^{k+1}(\boldsymbol{x}) \cdot \frac{\partial \boldsymbol{\varphi}_h(\boldsymbol{x})}{\partial x_s} \,\mathrm{d}\boldsymbol{x}. \tag{3.16}$$

The linearization of the term $\tilde{\sigma}_2$ can be carried out in a simple way, when $\boldsymbol{H}$ in (3.15) is chosen, for example, as the Vijayasundaram numerical flux, see [28], [15], Section 7.3 or [19], Section 3.3.4. The matrix $\boldsymbol{P}(\boldsymbol{w}, \boldsymbol{n})$ defined by (2.8) is diagonalizable: there exist matrices $\boldsymbol{D}$ and $\boldsymbol{T}$ such that

$$\boldsymbol{P}(\boldsymbol{w}, \boldsymbol{n}) = \boldsymbol{T}\boldsymbol{D}\boldsymbol{T}^{-1}, \;\; \boldsymbol{D} = \mathrm{diag}\;(\lambda_1, \dots, \lambda_4), \tag{3.17}$$

where $\lambda_1, \dots, \lambda_4$ are the eigenvalues of $\boldsymbol{P}$. We define the "positive" and "negative" part of $\boldsymbol{P}$ by

$$\boldsymbol{P}^{\pm}(\boldsymbol{w}, \boldsymbol{n}) = \boldsymbol{T}\boldsymbol{D}^{\pm}\boldsymbol{T}^{-1}, \;\; \boldsymbol{D} = \mathrm{diag}\;(\lambda_1^{\pm}, \dots, \lambda_4^{\pm}). \tag{3.18}$$

Then the Vijayasundaram numerical flux reads

$$\boldsymbol{H}_{VS}(\boldsymbol{w}_1, \boldsymbol{w}_2, \boldsymbol{n}) = \boldsymbol{P}^{+}\left(\frac{\boldsymbol{w}_1 + \boldsymbol{w}_2}{2}, \boldsymbol{n}\right)\boldsymbol{w}_1 + \boldsymbol{P}^{-}\left(\frac{\boldsymbol{w}_1 + \boldsymbol{w}_2}{2}, \boldsymbol{n}\right)\boldsymbol{w}_2. \tag{3.19}$$

The form of $\boldsymbol{H}_{VS}$ offers the linearized approximation

$$\begin{aligned} \tilde{\sigma}_2 \;\; \approx \;\; & \sum_{K_i \in \mathcal{T}_h} \sum_{j \in S(i)} \int_{\Gamma_{ij}} \Big[\boldsymbol{P}^{+}\left(\langle \boldsymbol{w}_h^k \rangle_{ij}, \boldsymbol{n}_{ij}\right) \boldsymbol{w}_h^{k+1}|_{\Gamma_{ij}} \\ & \qquad\qquad + \boldsymbol{P}^{-}\left(\langle \boldsymbol{w}_h^k \rangle_{ij}, \boldsymbol{n}_{ij}\right) \boldsymbol{w}_h^{k+1}|_{\Gamma_{ji}}\Big] \cdot \boldsymbol{\varphi}_h \mathrm{d}S, \end{aligned} \tag{3.20}$$

where

$$\langle \boldsymbol{w}_h^k \rangle_{ij} \equiv \frac{1}{2}\left(\boldsymbol{w}_h^k|_{\Gamma_{ij}} + \boldsymbol{w}_h^k|_{\Gamma_{ji}}\right). \tag{3.21}$$

It is necessary to specify the meaning of $\boldsymbol{w}_h^{k+1}|_{\Gamma_{ji}}$ for $\Gamma_{ij} \subset \partial\Omega_h$. If $j \in \gamma_{IO}(i)$, then we replace $\boldsymbol{w}_h^{k+1}|_{\Gamma_{ij}}$ in (3.20) by the state $\boldsymbol{w}_h^k|_{\Gamma_{ij}}$ determined in (3.7). For $j \in \gamma_W(i)$, in virtue of (3.8), we use the approximation

$$\boldsymbol{H}(\boldsymbol{w}_h^{k+1}|_{\Gamma_{ij}}, \boldsymbol{w}_h^{k+1}|_{\Gamma_{ji}}, \boldsymbol{n}_{ij}) \cdot \boldsymbol{\varphi}_h(\boldsymbol{x})\mathrm{d}S \approx \int_{\Gamma_{ij}} \boldsymbol{F}_W(\boldsymbol{w}_h^{k+1}, \boldsymbol{n}_{ij}) \cdot \boldsymbol{\varphi}\,\mathrm{d}S, \;\; j \in \gamma_W(i), \tag{3.22}$$

where $\boldsymbol{F}_W$ is given by (3.9). The vector $\boldsymbol{F}_W$ is a nonlinear function of $\boldsymbol{w}$ and its linearization can be carried out in two ways.

a) *Explicit way:* we simply put

$$\boldsymbol{F}_W(\boldsymbol{w}_h^{k+1}, \boldsymbol{n}) \approx \tilde{\boldsymbol{F}}_W(\boldsymbol{w}_h^k, \boldsymbol{w}_h^{k+1}) := \boldsymbol{F}_W(\boldsymbol{w}_h^k|_{\Gamma_{ij}}, \boldsymbol{n}). \tag{3.23}$$

This term appears on the right hand side of the resulting system of algebraic equations.

b) *Implicit way*: we use a linearization with the aid of the Taylor expansion as

$$\begin{aligned} \boldsymbol{F}_W(\boldsymbol{w}_h^{k+1}, \boldsymbol{n}) \approx \tilde{\boldsymbol{F}}_W(\boldsymbol{w}_h^k, \boldsymbol{w}_h^{k+1}) \;\; := \;\; & \boldsymbol{F}_W(\boldsymbol{w}_h^k, \boldsymbol{n}) \\ + \;\; & \frac{D\boldsymbol{F}_W(\boldsymbol{w}_h^k, \boldsymbol{n})}{D\boldsymbol{w}_h}\left(\boldsymbol{w}_h^{k+1} - \boldsymbol{w}_h^k\right). \end{aligned} \tag{3.24}$$

In the case a), $\tilde{\boldsymbol{F}}_W$ is independent of $\boldsymbol{w}_h^{k+1}|_{\Gamma_{ij}}$, whereas in the case b) it depends linearly on $\boldsymbol{w}_h^{k+1}|_{\Gamma_{ij}}$. The approach a) is simpler for implementation whereas the possibility b) allows to use a significantly higher CFL number in the stability condition specified in (3.32). In both cases a) and b) we put

$$
\begin{aligned}
\text{(3.25)} \qquad \sigma_2 \; = \; & \sum_{K_i \in \mathcal{T}_h} \sum_{j \in s(i)} \int_{\Gamma_{ij}} \Big[\boldsymbol{P}^+ \left(\langle \boldsymbol{w}_h^k \rangle_{ij}, \boldsymbol{n}_{ij} \right) \boldsymbol{w}_h^{k+1}|_{\Gamma_{ij}} \\
& \qquad + \boldsymbol{P}^- \left(\langle \boldsymbol{w}_h^k \rangle_{ij}, \boldsymbol{n}_{ij} \right) \boldsymbol{w}_h^{k+1}|_{\Gamma_{ji}} \Big] \cdot \boldsymbol{\varphi}_h \mathrm{d}S \\
+ \; & \sum_{K_i \in \mathcal{T}_h} \sum_{j \in \gamma_{IO}(i)} \int_{\Gamma_{ij}} \Big[\boldsymbol{P}^+ \left(\langle \boldsymbol{w}_h^k \rangle_{ij}, \boldsymbol{n}_{ij} \right) \boldsymbol{w}_h^{k}|_{\Gamma_{ij}} \\
& \qquad + \boldsymbol{P}^- \left(\langle \boldsymbol{w}_h^k \rangle_{ij}, \boldsymbol{n}_{ij} \right) \boldsymbol{w}_h^{k}|_{\Gamma_{ji}} \Big] \cdot \boldsymbol{\varphi}_h \mathrm{d}S \\
+ \; & \sum_{K_i \in \mathcal{T}_h} \sum_{j \in \gamma_W(i)} \int_{\Gamma_{ij}} \tilde{\boldsymbol{F}}_W(\boldsymbol{w}_h^k, \boldsymbol{w}_h^{k+1}, \boldsymbol{n}_{ij}) \cdot \boldsymbol{\varphi} \, \mathrm{d}S.
\end{aligned}
$$

Finally, we define the form

$$
\text{(3.26)} \qquad b_h(\boldsymbol{w}_h^k, \boldsymbol{w}_h^{k+1}, \boldsymbol{\varphi}_h) = -\sigma_1 + \sigma_2,
$$

where σ_1 and σ_2 are given by (3.16) and (3.25), respectively. The form b_h is linear with respect to the second and third variable. Using (3.14) and (3.26) we arrive at the following *semi-implicit linearized numerical scheme*: for each $k \geq 0$ find $\boldsymbol{w}_h^{k+1}$ such that

$$
\begin{aligned}
& \text{a) } \boldsymbol{w}_h^{k+1} \in [S_h]^4, \\
\text{(3.27) } & \text{b) } \left(\boldsymbol{w}_h^{k+1}, \boldsymbol{\varphi}_h \right) + \tau_k b_h(\boldsymbol{w}_h^k, \boldsymbol{w}_h^{k+1}, \boldsymbol{\varphi}_h) = \left(\boldsymbol{w}_h^k, \boldsymbol{\varphi}_h \right) \; \forall \, \boldsymbol{\varphi}_h \in [S_h]^4, \; k = 0, 1, \ldots, \\
& \text{c) } \boldsymbol{w}_h^0 = \Pi_h \boldsymbol{w}^0.
\end{aligned}
$$

3.4 Matrix representation

Let

$$
\text{(3.28)} \qquad \left\{ \boldsymbol{\varphi}_{imn} \in [S_h]^4; \; n = 1, \ldots, 4, \; m = 1, \ldots, DOF(p), \; i \in I \right\}
$$

be a basis of $[S_h]^4$. Here $DOF(p)$ denotes the number of degrees of freedom of functions $\phi \in S_h$ on one element $K \in \mathcal{T}_h$. For example, $DOF(0) = 1$ for a piecewise constant approximation (finite volume method), $DOF(1) = 3$ for a piecewise linear approximation, $DOF(2) = 6$ for a piecewise quadratic approximation, etc. Then the dimension of the space $[S_h]^4$ is $N = 4 \cdot DOF(p) \cdot \#\mathcal{T}_h$, where $\#\mathcal{T}_h$ denotes the number of elements of $\mathcal{T}_h$. The state vector $\boldsymbol{w}_h^k$ can be written in the form

$$
\text{(3.29)} \qquad \boldsymbol{w}_h^k(\boldsymbol{x}) = \sum_{i \in I} \sum_{m=1}^{DOF(p)} \sum_{n=1}^{4} \alpha_{imn}^k \boldsymbol{\varphi}_{imn}(\boldsymbol{x}), \quad \boldsymbol{x} \in \Omega, \; k = 0, 1, \ldots,
$$

where $\alpha_{imn}^k \in I\!R$. Then the numerical scheme (3.27) has the following matrix representation

$$
\text{(3.30)} \qquad \boldsymbol{M}(\boldsymbol{\alpha}^k) \boldsymbol{\alpha}^{k+1} = \boldsymbol{g}(\boldsymbol{\alpha}^k), \quad k = 0, 1, \ldots,
$$

where

$$
\text{(3.31)} \qquad \boldsymbol{\alpha}^k = \{ \alpha_{imn}^k \}_{l=1,\ldots,4, \; m=1,\ldots,DOF(p), \; i \in I} \in I\!R^N,
$$

$\boldsymbol{g} : I\!R^N \to I\!R^N$ and matrix $\boldsymbol{M}(\boldsymbol{\alpha})$ is an $N \times N$ matrix for each $\boldsymbol{\alpha} \in I\!R^N$. The solution of (3.30) can be obtained by a suitable solver for sparse nonsymmetric systems. (For the application of various linear solvers to the solution of inviscid flow with the finite volume method, see [22].)

In order to guarantee the stability of scheme (3.27), we use the following CFL condition

$$6\tau_k \max_{K_i \in \mathcal{T}_h} \frac{1}{|K_i|} \left(\max_{j \in S(i)} |\Gamma_{ij}| \lambda^{\max}_{\boldsymbol{P}(\boldsymbol{w}_h^k|_{\Gamma_{ij}}, \boldsymbol{n}_{ij})} \right) \leq \text{ CFL}, \tag{3.32}$$

where $|K_i|$ denotes the area of K_i, $|\Gamma_{ij}|$ the length of the edge Γ_{ij}, CFL a given constant and $\lambda^{\max}_{\boldsymbol{P}(\boldsymbol{w}_h^k|_{\Gamma_{ij}}, \boldsymbol{n}_{ij})}$ is the maximal eigenvalue of the matrix $\boldsymbol{P}(\boldsymbol{w}_h^k|_{\Gamma_{ij}}, \boldsymbol{n}_{ij})$ defined in (2.8), where the maximum is taken over Γ_{ij}. The condition (3.32) is similar to the stability condition widely used in the finite volume method, obtained on the basis of linearization and in analogy with a scalar problem, see [15], Section 7.3 or [19], Section 3.3.7. For a detailed treatment of various approaches to the stability investigation, see also [29], Chapters 5 and 9. In contrast to explicit schemes, for which we have to choose CFL < 1 ([10]), the semi-implicit scheme (3.27) allows us to use CFL ≈ 6 for the linearization (3.23) and CFL ≈ 100 for the linearization (3.24), as is established by numerical experiments, see Section 5. Hence, the semi-implicit linearized schemes allow us to choose much longer time step than the explicit scheme.

4 Implementation

The computations presented in this paper were performed on triangular grids with the aid of piecewise linear approximations, i. e. with $p = 1$ in (3.11).

The volume integrals in (3.16) are evaluated by the three point integration rule

$$\int_{K_i} z(\boldsymbol{x})\,\mathrm{d}\boldsymbol{x} \approx \frac{1}{3}|K_i| \sum_{j \in S(i)} z(Q_{ij}), \tag{4.1}$$

where $|K_i|$ denotes the area of K_i and Q_{ij}, $j \in S(i)$, denotes the midpoint of the edge Γ_{ij}. This integration rule is exact for second degree polynomials. The integrals in (3.25) are evaluated by the two points Gauss quadrature rule

$$\int_{\Gamma_{ij}} z\,\mathrm{d}S \approx \frac{|\Gamma_{ij}|}{2} \left(z(Q^1_{ij}) + z(Q^2_{ij}) \right), \tag{4.2}$$

where $|\Gamma_{ij}|$ denotes the length of the edge Γ_{ij} and Q^1_{ij} and Q^2_{ij} are integration points lying on Γ_{ij}. Let Γ_{ij} be parameterized in the form

$$\Gamma_{ij} = \left\{ \boldsymbol{x} \in I\!R^2,\ \boldsymbol{x} = \boldsymbol{c}_{ij} + s(\boldsymbol{d}_{ij} - \boldsymbol{c}_{ij}),\ s \in [0,1] \right\}, \tag{4.3}$$

where $\boldsymbol{c}_{ij}$ and $\boldsymbol{d}_{ij}$ are endpoints of Γ_{ij}. Then

$$\begin{aligned} Q^1_{ij} &= \boldsymbol{c}_{ij} + \left(1 - \sqrt{3}/3\right)(\boldsymbol{d}_{ij} - \boldsymbol{c}_{ij})/2, \\ Q^2_{ij} &= \boldsymbol{c}_{ij} + \left(1 + \sqrt{3}/3\right)(\boldsymbol{d}_{ij} - \boldsymbol{c}_{ij})/2. \end{aligned} \tag{4.4}$$

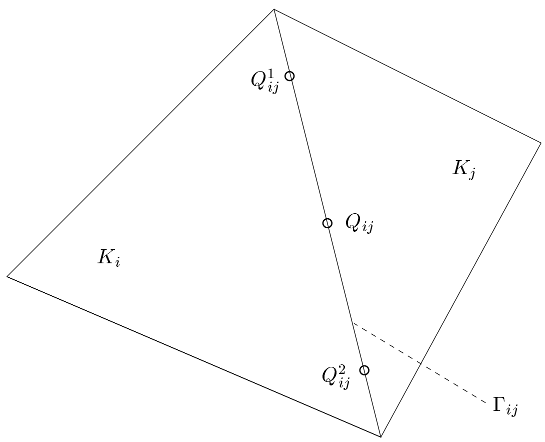

Figure 1: Integration nodes Q_{ij}, Q_{ij}^1 and Q_{ij}^2 of the edge Γ_{ij}

The approximation (4.2) is exact for polynomials of the third degree. As we see, for each edge Γ_{ij}, $j \in S(i)$, $i \in I$, we have to evaluate the state vector $\boldsymbol{w}$ at three integration nodes: Q_{ij}, Q_{ij}^1 and Q_{ij}^2, see Figure 1.

There are two natural possibilities how to choose the basis (3.28) of the space $[S_h]^4$. First, let us consider basis functions associated with vertices of the triangulation $\mathcal{T}_h$. Then we can write

$$
\begin{aligned}
(4.5)\qquad \boldsymbol{\varphi}_{imn} = (\phi_{im}\delta_{n1}, \dots, \phi_{im}\delta_{n4}),\ \phi_{im} \in S_h, \phi_{im}(P_{i'}^{m'}) = \delta_{ii'}\delta_{mm'},& \\
m' = 1,2,3\ i' \in I,\ n = 1,\dots,4,\ m = 1,2,3,\ i \in I,&
\end{aligned}
$$

where P_i^m, $m = 1,2,3$, are vertices of the triangle K_i. The use of the basis (4.5) leads to a 7-points stencil for every test function and hence, the matrix $\boldsymbol{M}$ has at most 28 nonzero elements in each row, see Figure 2.

The second possibility is to consider basis functions, whose components are piecewise linear functions associated with *midpoints of edges of triangles*:

$$
\begin{aligned}
(4.6)\qquad \boldsymbol{\varphi}_{imn} = (\phi_{im}\delta_{n1}, \dots, \phi_{im}\delta_{n4}),\ \phi_{im} \in S_h, \phi_{im}(Q_{i'}^{m'}) = \delta_{ii'}\delta_{mm'},& \\
m' = 1,2,3\ i' \in I,\ n = 1,\dots,4,\ m = 1,2,3,\ i \in I,&
\end{aligned}
$$

where Q_i^m, $m = 1,2,3$, are midpoints of edges of element K_i (of course, $Q_i^m = Q_{ij}$ for some $j \in S(i)$). The choice (4.6) leads to a 12-points stencil for any test function and the matrix $\boldsymbol{M}$ has at most 48 nonzero elements in each row, see Figure 2.

As we see, the choice (4.5) produces significantly smaller number (about 57 %) of nonzero elements than the choice (4.6). This is caused by the fact that each function ϕ_{im} from (4.5) has a zero trace along one edge of K_i and, moreover, for the evaluation of $\boldsymbol{w}$ at Q_{ij}^1 and Q_{ij}^2 only the values of $\boldsymbol{w}$ at endpoints of Γ_{ij} are used (not the value at the third vertex of K_i, see Figure 2).

The linear system (3.30) is solved by the GMRES method ([25]), in which the vector $\boldsymbol{\alpha}^k$ is taken as an initial approximation of $\boldsymbol{\alpha}^{k+1}$. Since we solve a time dependent problem, the vectors $\boldsymbol{\alpha}^k$ and $\boldsymbol{\alpha}^{k+1}$ are close each other (especially when we seek a steady state solution)

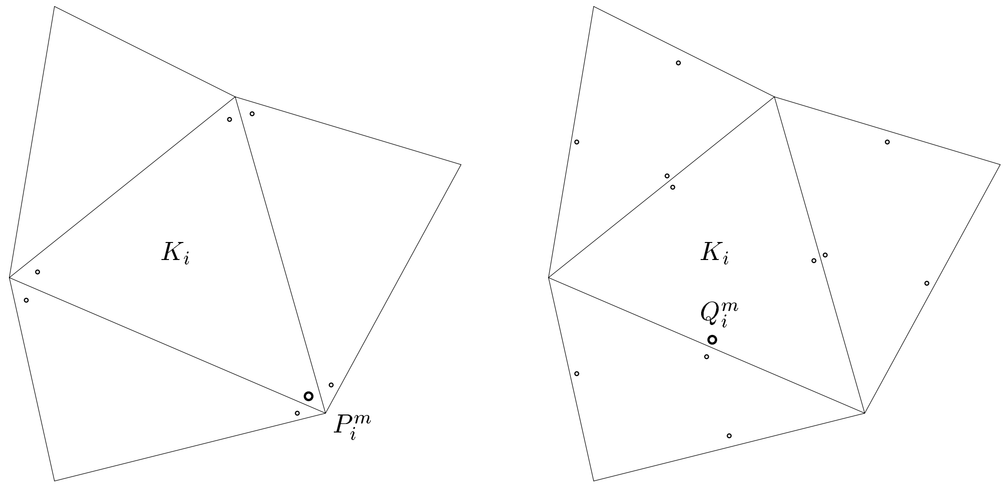

Figure 2: Seven point stencil of a node P_i^m (left) and twelve point stencil of a node Q_i^m.

and, therefore, only few GMRES iterations at each time step are necessary. This is the reason that GMRES method can be used without any preconditioning.

Condition (3.32) guarantees the stability of the scheme with CFL $\gg 1$. On the other hand, the computations start often from nonphysical data in the initial condition (2.5) (for example, we choose, $\boldsymbol{w}^0(\boldsymbol{x})$ as a constant vector for all $\boldsymbol{x} \in \Omega$). Consequently, it is suitable to start the computation process with a smaller CFL number (in order to avoid physically unacceptable situations, as, for example, negative pressure) and then, step by step to increase CFL.

Numerical experiments show (see, e.g., [2], [3], [10], [21]) that in order to obtain a physically admissible numerical solution, the use of superparametric finite elements is required. This means that the elements K adjacent to a curved boundary have to be approximated by elements $\tilde{K}$ which are images of a reference element $\hat{K}$ in a polynomial mapping $\zeta : \hat{K} \overset{\text{onto}}{\to} K$ having a higher degree than the degree of functions from the space S_h. Namely, in our case of linear finite elements, it is sufficient to employ a bilinear mapping ζ, see [10].

If the sought solution contains discontinuities (shock waves or contact discontinuities) then overshoots and undershoots appear in the DGFE solution near the discontinuities. To avoid this phenomenon, it is necessary to decrease the order of accuracy of the method choosing $p = 0$ in the vicinity of the discontinuities. One possibility, which is quite reliable, is to use the automatic adaptive limiting of order of accuracy proposed in [13].

5 Numerical examples

We present the results obtained for the Ringleb flow problem. In this test case an analytical smooth steady-state solution of the Euler equations was obtained with the aid of the "hodograph method", see [5]. This problem represents a transonic channel flow, which is mostly subsonic, with a small supersonic region near the right-hand side wall,

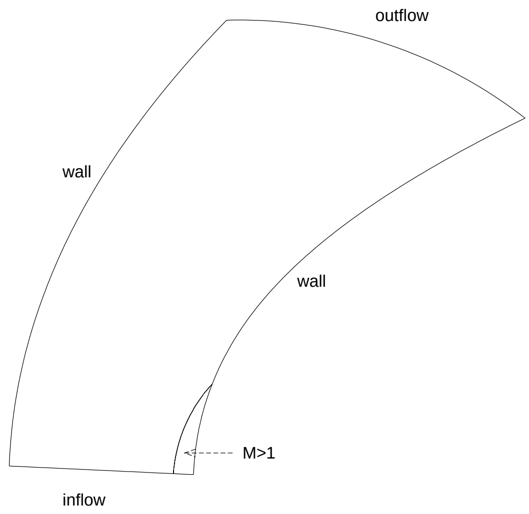

Figure 3: Geometry for Ringleb flow problem with marked supersonic region

as shown in Figure 3. Our aim is to obtain the approximate DG steady state solution and compare it with the analytical one. On both walls we prescribed the impermeability condition $\boldsymbol{v} \cdot \boldsymbol{n} = 0$ where $\boldsymbol{n}$ denotes the outer normal to $\partial\Omega$. On the inflow and outflow parts of the boundary we prescribe the exact solution. As an initial condition (2.5) we have chosen a constant vector $\boldsymbol{w}^0 = (0.5, 0, 0, 0.5)$.

The steady-state solution is achieved by a time stabilization method for "$t \to \infty$" with the aid of the forward Euler time discretization and the semi-implicit method (3.27) using linearizations (3.23) and (3.24) of fluxes. The stopping criterion is given by

$$\max\left(1, \frac{1}{\tau_k}\right) \left\|\rho_h^{k+1} - \rho_h^k\right\|_{L^1(\Omega)} \leq \mathrm{TOL}, \tag{5.7}$$

where ρ_h^{k+1} and ρ_h^k denote the density at time levels t_{k+1} and t_k, respectively, $\tau_k = t_{k+1} - t_k$ and TOL is a given tolerance. We put $\mathrm{TOL} = 10^{-6}$ for computations presented in this paper.

The goal of our numerical experiments is to establish the order of accuracy and to compare the efficiency (CPU time) of the presented methods. The computations are performed for 4 triangular grids $\mathcal{T}_{h_l}$, $l = 1, \dots, 4$, having 5×10, 10×20, 20×40 and 40×80 vertices, see Figure 4. Since the corresponding isolines of Mach number obtained by all mentioned methods are identical, we show only results obtained by the semi-implicit scheme with the linearization (3.24), which are viewed on Figure 5. We observe a very smooth resolution although the discontinuous approximation was employed. Table 1 shows the computational errors e_h for explicit as well as semi-implicit methods, defined by

$$e_h^2 \equiv \|\boldsymbol{w}_h - \boldsymbol{w}\|^2_{[L^2(\Omega_h)]^4}, \tag{5.8}$$

where $\boldsymbol{w}$ is the exact solution of the Ringleb flow problem and $\boldsymbol{w}_h$ is its numerical approximation on a mesh $\mathcal{T}_h$. Table 1 also contains the experimental order of convergence

method mesh	explicit e_h	α_l	semi-implicit+(3.23) e_h	α_l	semi-implicit+(3.24) e_h	α_l
5×10	7.85E-03	–	7.40E-03	–	7.81E-03	–
10×20	1.51E-03	2.05	1.45E-03	2.03	1.51E-03	2.05
20×40	3.41E-04	2.01	3.30E-04	2.00	3.39E-04	2.01
40×80	7.86E-05	2.04	7.71E-05	2.03	7.85E-05	2.04

Table 1: Computational errors in L^2-norm and corresponding experimental order of accuracy for explicit and semi-implicit methods

method mesh	explicit #steps	CPU (s)	semi-implicit+(3.23) #steps	CPU(s)	semi-implicit+(3.24) #steps	CPU(s)
5×10	7855	17.3	722	3.2	74	0.6
10×20	22909	136.0	1820	36.9	166	6.7
20×40	51963	1046.3	4826	376.9	561	126.7
40×80	116364	8565.1	10872	3666.4	1262	905.6

Table 2: Number of time steps (#steps) and CPU time for explicit and semi-implicit methods

given by

$$\alpha_l = \frac{\log\left(e_{h_l}/e_{h_{l-1}}\right)}{\log\left(h_l/h_{l-1}\right)}, \quad l = 2, \dots, 4, \tag{5.9}$$

where h_l is the mesh size of $\mathcal{T}_{h_l}$ and e_{h_l} is the corresponding computational error achieved on this mesh. All methods have the experimental order of convergence equal to 2, which corresponds to optimal approximation properties of linear finite elements.

Table 2 compares the number of time steps and CPU time measured in seconds for all three methods. The number of time steps necessary for the time stabilization satisfying the criterion (5.7) is about 10 times and 100 times smaller for semi-implicit method with (3.23) and (3.24) than for the explicit one, respectively. This corresponds to the choice of the CFL-number in the stability condition (3.32): CFL=0.6 for the forward Euler scheme, whereas CFL=6 and CFL=100 for the semi-implicit methods using (3.23) and (3.24), respectively, (see Section 3.4). The GMRES solution of system (3.30) needs some additional computational costs, but Table 2 shows that the total CPU-time is significantly smaller for semi-implicit schemes. (The computation was performed on PC Intel P4, 2.4GHz.)

6 Conclusion

We present efficient higher order numerical schemes for the solution of the Euler equations using the discontinuous Galerkin finite element space discretization. In order to avoid a time step restriction known from explicit methods, semi-implicit numerical schemes were developed. The main tool is the linearization of the flux and numerical flux leading to the solution of a linear algebraic system at each time level. In our schemes we use the

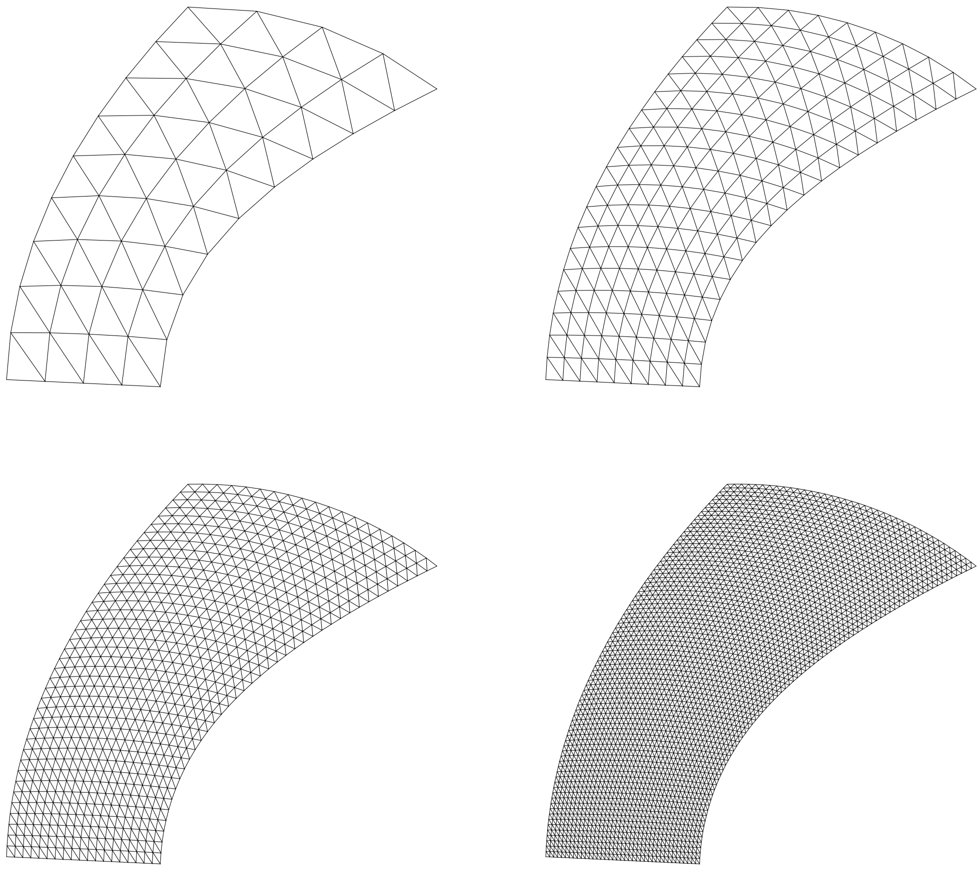

Figure 4: Grids used for the Ringleb flow problem with 5×10, 10×20, 20×40 and 40×80 vertices

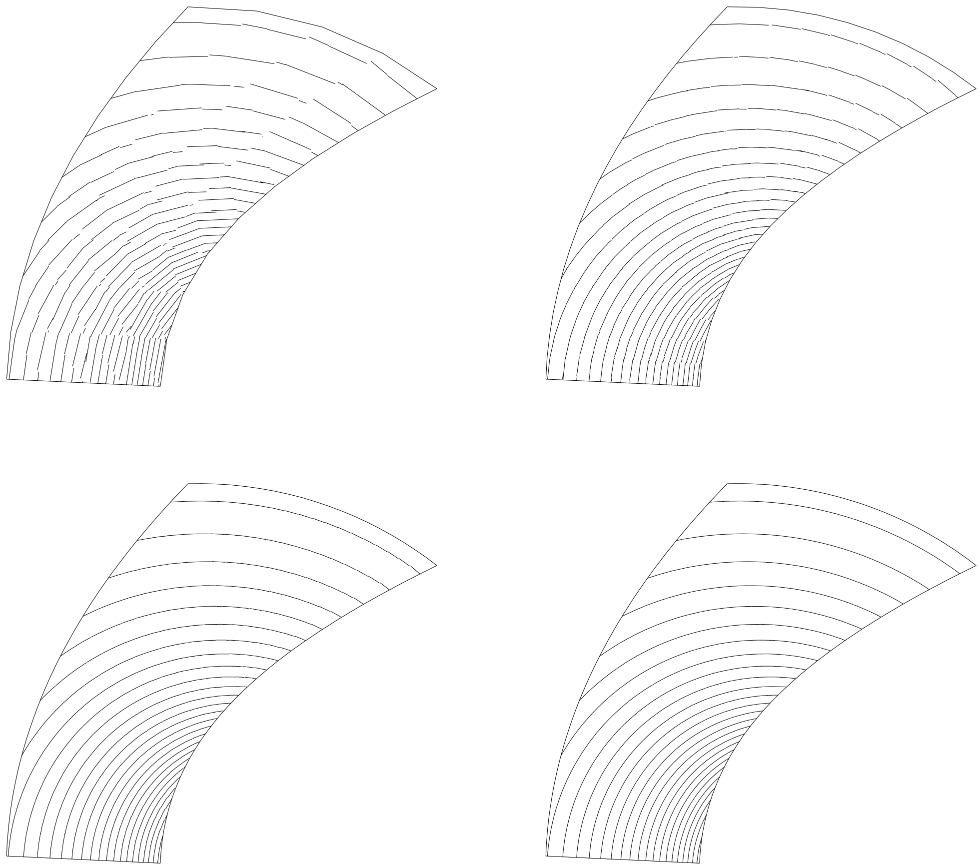

Figure 5: Ringleb flow problem: computed isolines of Mach number obtained by the semi-implicit scheme on grids with 5×10, 10×20, 20×40 and 40×80 vertices

Vijayasundaram numerical flux, which is suitable for linearization. An important issue is the linearization of boundary conditions. We introduce here two versions – fully explicit and implicit. Our further goal was the investigation of the accuracy and efficiency of the developed schemes. Numerical experiments performed for the Ringleb flow problem confirm that the order of accuracy of discontinuous piecewise linear approximations (for semi-implicit as well as explicit schemes) is equal to 2. Thus, the order of accuracy is optimal. Moreover, the semi-implicit schemes allow to use much larger CFL-number than the explicit one. This results among other in a strong reduction of the computer time necessary for obtaining a steady-state solution of the Euler equations with the use of the time stabilization for "$t \to \infty$".

Acknowledgments We wish to express our sincere gratitude to Professor Tim Barth (NASA Ames Research Center) for providing the algorithm for generating the analytical solution to Ringleb flow and Paul Houston (University of Leicester) for providing the GMRES algorithm.

References

[1] S. Adjerid, D. Devine, J. E. Flaherty, and L. Krivodonova. A posteriori error estimation for discontinuous Galerkin solutions of hyperbolic problems. *Comput. Methods Appl. Mech. Engrg.*, 191:1097–1112, (2002).

[2] F. Bassi and S. Rebay. High-order accurate discontinuous finite element solution of the 2D Euler equations. *J. Comput. Phys*, 138:251–285, (1997).

[3] F. Bassi and S. Rebay. A high order discontinuous Galerkin method for compressible turbulent flow. In B. Cockburn, G. E. Karniadakis, and C.-W. Shu, editors, *Discontinuous Galerkin Method: Theory, Computations and Applications*, Lecture Notes in Computational Science and Engineering 11, pages 113–123. Springer-Verlag, (2000).

[4] M. Bejček, V. Dolejší, and M. Feistauer. On discontinuous Galerkin method for numerical solution of conservation laws and convection–diffusion problems. In *Proceedings of the XIV Summer School Software and Algorithms of Numerical Mathematics*, pages 7–32, (2002).

[5] G. Chiocchia. Exact solutions to transonic and superesonic flows. Technical Report AGARD-AR-211, Center for Aerospace Information, NASA, (1985).

[6] B. Cockburn. Discontinuous Galerkin methods for convection dominated problems. In T. J. Barth and H. Deconinck, editors, *High–Order Methods for Computational Physics*, Lecture Notes in Computational Science and Engineering 9, pages 69–224. Springer, Berlin, (1999).

[7] B. Cockburn, S. Hou, and C. W. Shu. TVB Runge–Kutta local projection discontinuous Galerkin finite element for scalar conservation laws II: General framework. *Math. Comp.*, 52:411–435, (1989).

[8] B. Cockburn, G. E. Karniadakis, and C.-W. Shu (eds.). Discontinuous Galerkin methods. In *Lecture Notes in Computational Science and Engineering 11*. Springer, Berlin, (2000).

[9] V. Dolejší. A higher order scheme based on the finite volume approach. In R. Herbin and D. Kröner, editors, *Finite Volumes for Complex Applications III (Problems and Perspectives)*, pages 333–340. Hermes, (2002).

[10] V. Dolejší and M. Feistauer. The use of discontinuous Galerkin method for the numerical solution of convection–dominated problems. In F. Brezzi, A. Buffa, S. Corsaro, and A. Murli, editors, *Numerical Mathematics and Advanced Applications, ENUMATH 2001*, pages 65–84. Springer-Verlag, Italia, (2003).

[11] V. Dolejší, M. Feistauer, and C. Schwab. A finite volume discontinuous Galerkin scheme for nonlinear convection–diffusion problems. *Calcolo*, 39:1–40, (2002).

[12] V. Dolejší, M. Feistauer, and C. Schwab. On discontinuous Galerkin methods for nonlinear convection–diffusion problems and compressible flow. *Mathematica Bohemica*, 127(2):163–179, (2002).

[13] V. Dolejší, M. Feistauer, and C. Schwab. On some aspects of the discontinuous Galerkin finite element method for conservation laws. *Mathematics and Computers in Simulation*, 61:333–346, (2003).

[14] R. Eymard, T. Gallouët, and R. Herbin. *Solution of equations in R^n (Part 3). Techniques of scientific computing (Part 3).*, volume t of *Handbook of numerical analysis*, chapter Finite volume methods, pages 713–1–20. Amsterdam: North-Holland/ Elsevier, (2000).

[15] M. Feistauer. *Mathematical Methods in Fluid Dynamics.* Longman Scientific & Technical, Harlow, (1993).

[16] M. Feistauer. Discontinuous Galerkin method: Compromise between FV and FE schemes. In R. Herbin and D. Kröner, editors, *Finite Volumes for Complex Applications III (Problems and Perspectives)*, pages 81–95. Hermes, (2002).

[17] M. Feistauer and J. Felcman. Convection-diffusion problems and compressible Navier–Stokes equations. In J. R. Whitemen (ed.), *The Mathematics of Finite Elements and Applications*, pages 175–194. John Wiley & Sons, (1996).

[18] M. Feistauer, J. Felcman, and V. Dolejší. Numerical simulation of compresssible viscous flow through cascades of profiles. *ZAMM*, 76(S4):297–300, (1996).

[19] M. Feistauer, J.Felcman, and I. Straškraba. *Mathematical and Computational Methods for Compressible Flow.* Oxford University Press, Oxford, (2003).

[20] J. Felcman and P. Šolín. On the construction of the Osher–Solomon scheme for 3D Euler equations. *East–West J. Numer. Math.*, 6(1):43–64, (1998).

[21] R. Hartmann and P. Houston. Adaptive discontinuous Galerkin finite element methods for nonlinear hyperbolic conservation laws. *SIAM J. Sci. Comp.*, 24:979–1004, (2002).

[22] A. Meister: Comparison of different Krylov subspace methods embedded in an implicit finite volume scheme for the computation of viscoud and inviscid flow fields un unstructured grids. *J. Comput. Phys.*, 140:311–345, (1998).

[23] D. Kröner. *Numerical Schemes for Conservation Laws.* Wiley Teubner, Stuttgart, (1997).

[24] S. Osher and F. Solomon. Upwind difference schemes for hyperbolic systems of conservation laws. *Math. Comp.*, 38:339–374, (1982).

[25] Y. Saad and M. H. Schultz. GMRES: A generalized minimal residual algorithm for solving nonsymmetric linear systems. *SIAM J. Sci. Stat. Comput.*, 7:856–869, (1986).

[26] S. P. Spekreijse. Multigrid Solution of the Steady Euler Equations. Centre for Mathematics and Computer Science, Amsterodam, (1988).

[27] E. F. Toro. *Riemann Solvers and Numerical Methods for Fluid Dynamics.* Springer-Verlag, (1997).

[28] G. Vijayasundaram. Transonic flow simulation using upstream centered scheme of Godunov type in finite elements. *J. Comput. Phys.*, 63:416–433, (1986).

[29] P. Wesseling. *Principles of Computational Fluid Dynamics.* Springer, (2001).

List of preprints released in this series

All preprints available on http://www.karlin.mff.cuni.cz/ms-preprints/
E-mail contact to series administrator: knm-prep@karlin.mff.cuni.cz

[MATH-kma-2003/94] Jan Lang, Ales Nekvinda, Lubos Pick: *Boundedness and compactness of general kernel integral operators from a weighted Banach function space into* L_∞ (03.01.2003)

[MATH-alg-2003/1] R. El Bashir and T. Kepka: *Dually steady rings* (07.01.2003)

[MATH-alg-2003/2] S.Holub: *Binary equality languages for periodic morphisms* (07.01.2003)

[MATH-kma-2003/95] Jakub Duda: *On the size of the set of points where the metric projection exists* (13.01.2003)

[MATH-kma-2003/96] Ludek Zajicek, Miroslav Zeleny: *On complexity of a* σ*-ideal of* σ*-P-porous sets* (13.01.2003)

[MATH-kma-2003/97] Josef Danecek, Oldrich John, Jana Stara: *Interior* $C^{1,\gamma}$*-regularity for weak solutions of nonlinear second order elliptic systems* (13.01.2003)

[MATH-knm-2003/1] V. Dolejsi, M.Feistauer: *Discontinuous Galerkin finite element-method for convection-diffusion problemsand the compressible Navier–Stokes equations* (22.01.2003)

[MATH-kma-2003/98] Ralph Chill, Eva Fasangova: *Convergence to steady states of solutions of semilinear evolutionary integral equations* (25.01.2003)

[MATH-kma-2003/99] Jan Rychtar: *Pointwise uniformly rotund norms* (02.02.2003)

[MATH-kma-2003/100] Petr Holicky, Miklos Laczkovich: *Descriptive properties of the set of exposed points of compact convex sets in* R^3 (03.02.2003)

[MATH-kma-2003/101] Petr Holicky, Tamas Keleti: *Borel classes of sets of extreme and exposed points in* R^n (03.02.2003)

[MATH-alg-2003/3] Lidia Angeleri Hgel, Dolors Herbera and JanTrlifaj: *Tilting modules and Gorenstein rings* (28.02.2003)

[MATH-kma-2003/102] Robert Cerny: *Local monotonicity of measures supported by graphs of convex functions* (07.03.2003)

[MATH-kma-2003/103] Jan Maly: *Coarea integration in metric spaces* (07.03.2003)

[MATH-kma-2003/104] J. Lukes, T. Mocek, M. Smrcka, J. Spurny: *Choquet like sets in function spaces* (07.03.2003)

[MATH-kma-2003/104] J. Lukes, T. Mocek, M. Smrcka, J. Spurny: *Choquet like sets in function spaces* (07.03.2003)

[MATH-kma-2003/105] Jiri Spurny: F_σ*-additive families and the invariance of Borel classes* (22.03.2003)

[MATH-MU-2003/1] Jan Rataj: *On boundaries of unions of sets with positive reach* (28.03.2003)

[MATH-kma-2003/106] Dalibor Prazak: *A necessary and sufficient condition for the existence of an exponential attractor* (23.04.2003)

[MATH-kma-2003/107] Petr Hajek, Michal Johanis: *Smooth approximations without critical points* (23.04.2003)

[MATH-kma-2003/108] Petr Hajek, Michal Johanis: *A characterization of reflexivity* (28.04.2003)

[MATH-kma-2003/109] Ondrej Kalenda, Matias Raja: *Descriptive properties of spaces of signed measures* (04.05.2003)

[MATH-alg-2003/4] S.Holub: *A proof of Duval's conjecture* (05.05.2003)

[**MATH-kma-2003/110**] Miroslav Husek: $C_p(X)$ *in coreflective classes of locally convex spaces* (17.05.2003)

[**MATH-alg-2003/5**] A.Drapal: *Structural interactions of conjugacy closed loops* (26.05.2003)

[**MATH-alg-2003/6**] L. Bican: *Relatively exact modules* (26.05.2003)

[**MATH-kma-2003/111**] Petr Holicky, Jiri Spurny: F_s*igma-mappings and the invariance of absolute Borel classes* (28.05.2003)

[**MATH-kma-2003/112**] Eva Fasangova, Pedro J. Miana: *Spectral mapping inclusions for the Phillips functional calculus in Banach spaces and algebras* (28.05.2003)

[**MATH-kma-2003/113**] Ondrej Kalenda: *Note on countable unions of Corson countably compact spaces* (28.05.2003)

[**MATH-kma-2003/114**] Stanislav Hencl, Jan Maly: *Absolutely continuous functions of several variables and diffeomorphisms* (25.06.2003)

[**MATH-MU-2003/2**] Jan Rataj: *On estimation of the Euler number by projections on thin slabs* (28.07.2003)

[**MATH-alg-2003/7**] Jan Trlifaj, Paul C. Eklof, and Saharon Shelah: *On the cogeneration of cotorsion pairs* (29.07.2003)